J Mater Sci (2010) 45:3413–3418
DOI 10.1007/s10853-010-4366-y

Yttrium-doped nanocrystalline Ni_4Mo: ultrahigh strength and high ductility combined with useful intermetallic properties

H. M. Tawancy · M. O. Aboelfotoh

Received: 18 December 2009 / Accepted: 1 March 2010 / Published online: 9 March 2010

Abstract We show that bulk nanocrystalline Ni_4Mo can be synthesized by doping with small but critical concentrations of Y. Two alloys are included in the study with compositions of Ni_4Mo and Ni_4Mo + 0.01 wt% Y. Microstructural features derived from transmission electron microscopy observations are correlated with room-temperature tensile properties. Yttrium-doped Ni_4Mo is found to have room-temperature yield strength in excess of 800 MPa and tensile elongation to failure of about 40% while simultaneously retaining other useful physical and chemical properties of intermetallic compounds. Twinning rather than slip is found to be the predominant deformation mechanism, which is correlated with the superlattice structure of Ni_4Mo. Since deformation by twinning is polarized, this is expected to enhance the fatigue life.

Introduction

Nanocrystalline materials with ultrahigh strength and high ductility offer a huge potential for high performance structural applications. Although a considerable progress has been made toward fabricating these materials by severe plastic deformation [1–3], the relatively low ductility particularly at ambient temperatures remains to be an important issue [4–6] analogous to intermetallic compounds [7]. However, in recent years, the number of intermetallic compounds discovered to have relatively high ductility continues to increase [8–11]. Therefore, intermetallic compounds are expected to have an important share of future generations of structural materials.

Recently, we have shown that nanocrystalline superlattice of $Ni_2(Mo,Cr)$ can be synthesized with ultrahigh strength and high ductility [8, 9]. Although Ni_2Mo is thermodynamically metastable in the Ni–Mo system [12], we have found that it can be stabilized by critical additions of Cr depending upon the exact Mo content [13]. Also, we have shown that the small but critical additions of Y can improve the thermal stability characteristics of ordered Ni–Mo alloys [14]. The objective of this paper is to show that bulk nanocrystalline Ni_4Mo with potentially useful combination of properties can be synthesized by doping with small but critical concentrations of Y.

Experimental procedure

The two alloys included in the study have chemical compositions in weight percentage of Ni–29.05Mo (Ni_4Mo) and Ni–29.12Mo + 0.01Y (Ni_4Mo + Y). Both alloys were processed by vacuum melting, hot rolling, and cold rolling into sheets about 3 mm in thickness. Test samples were fully recrystallized by an annealing heat treatment at 1065 °C followed by water quenching. It is known that below about 870 °C, the parent disordered face-centered cubic lattice (fcc) of Ni_4Mo transforms into the body-centered tetragonal $D1_a$ superlattice, e.g., Ref. [15]. Thermal aging of annealed samples was carried out for up to 1000 h at 700 °C where ordering is found to occur most rapidly. Tensile tests were carried out at room temperature

H. M. Tawancy (✉)
Center for Engineering Research and Center for Research Excellence in Corrosion, Research Institute, King Fahd University of Petroleum & Minerals, P.O. Box 1639, Dhahran 32161, Saudi Arabia
e-mail: tawancy@kfupm.edu.sa

M. O. Aboelfotoh
Department of Materials Science and Engineering, North Carolina State University, Raleigh, NC 27606, USA

on standard samples with a gage length of 50.8 mm. Both the linear coefficient of thermal expansion and corrosion rate in boiling 20% hydrochloric acid were measured in the disordered and fully ordered conditions. Transmission electron microscopy was used to characterize the microstructure. All crystallographic notations are given in terms of the parent fcc lattice.

Experimental results and discussion

On the scale of light optical metallography, the two alloys are observed to consist of equiaxed grains with high density of annealing twins suggesting relatively low stacking fault energy as shown in Fig. 1a. However, on the finer scale of transmission electron microscopy, some of the {111} annealing twins observed in Fig. 1a, are found to be subdivided into smaller coherent twins with a nanoscale width as illustrated in Fig. 1b. It is shown later that long-range ordering divides each grain shown in Fig. 1a into an aggregate of f nanoscale particles. Since Mo is known to reduce the stacking fault energy of Ni [15, 16], this could enhance the tendency for twinning. As shown later, most of the twinning systems in the fcc lattice are preserved in the $D1_a$ superlattice and therefore, the nanoscale twins observed in Fig. 1b are expected to act as source of strengthening. As expected, both alloys are observed to contain short-range order indicated by the appearance of diffuse intensity maxima at ⟨1 1/2 0⟩ and all equivalent positions as shown in the ⟨001⟩ diffraction pattern of Fig. 1c. A corresponding high-resolution TEM image is shown in Fig. 1d, which can be interpreted in terms of subunit cell clusters of the crystallographically related $D1_a$ (Ni_4Mo), DO_{22} (Ni_3MO), and Pt_2Mo-type (Ni_2Mo) superlattices using a multi-slice image simulation model [17]. This is consistent with the finding that the three superlattices have similar ground-state energy [18]. The relative stability of each superlattice is dependent upon the exact chemical composition as pointed out earlier.

Comparative true stress–strain diagrams derived at room temperature are shown in Fig. 2. In the fully ordered condition, the 0.2% yield strength of both alloys is nearly doubled relative to the as-quenched condition (short-range ordered). However, the undoped Ni_4Mo is observed to have less than 5% tensile elongation to failure, while the Y-doped Ni_4Mo is able to maintain about 40% elongation. Also, the Y-doped alloy exhibits lower strain hardening rate in comparison with the as-quenched condition, which

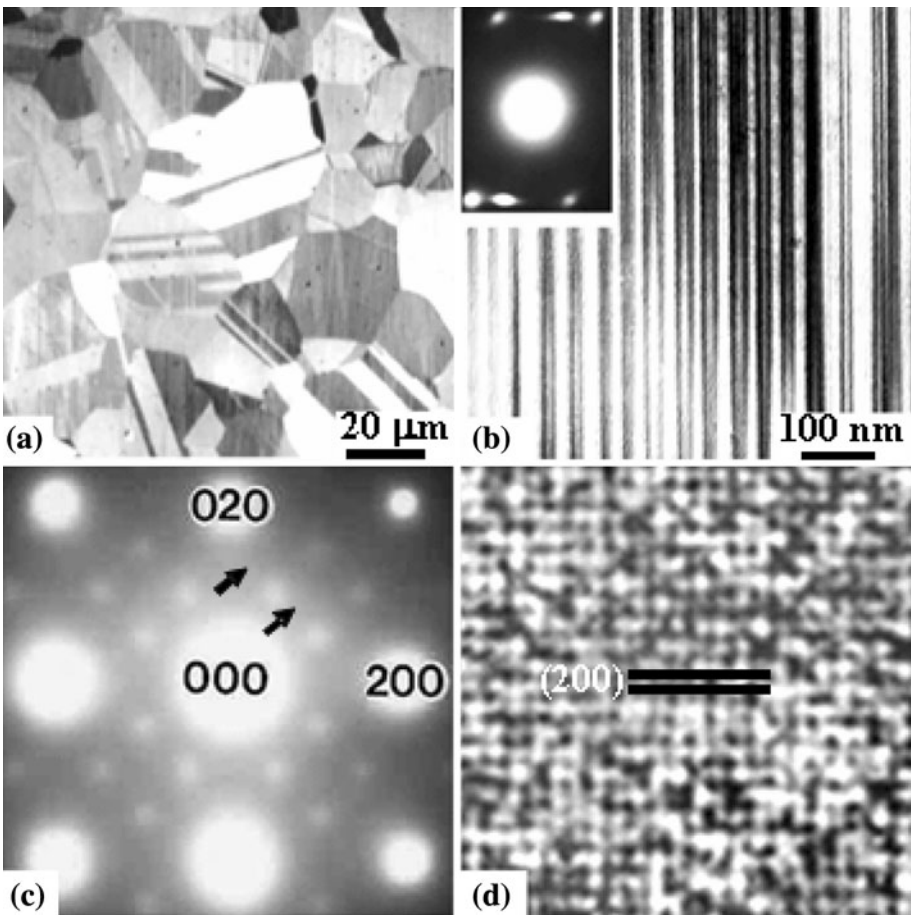

Fig. 1 Characteristic microstructural features of Ni_4Mo alloy in the as-quenched condition. **a** Optical micrograph of the grain structure. **b** Bright-field TEM image of nanoscale twins and corresponding ⟨110⟩ twin diffraction pattern. **c** ⟨001⟩ diffraction pattern showing short-range order reflections at ⟨1 1/2 0⟩ positions. **d** Corresponding high-resolution TEM image

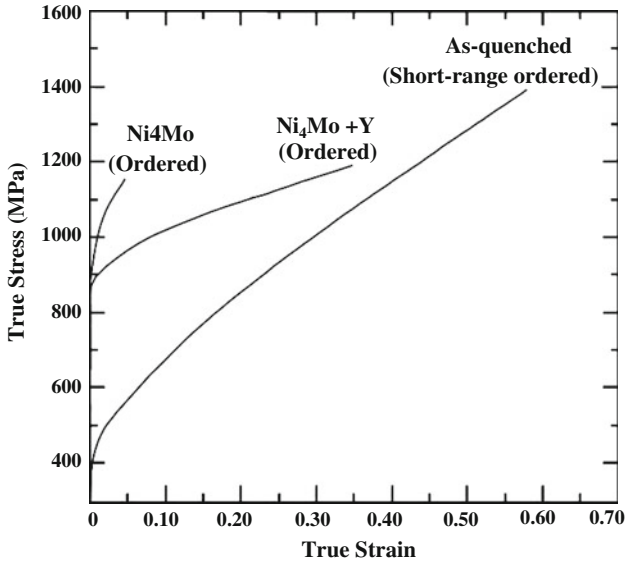

Fig. 2 Comparative true tensile stress–strain diagrams showing the effect of thermal aging for 1440 min at 700 °C on room-temperature tensile properties

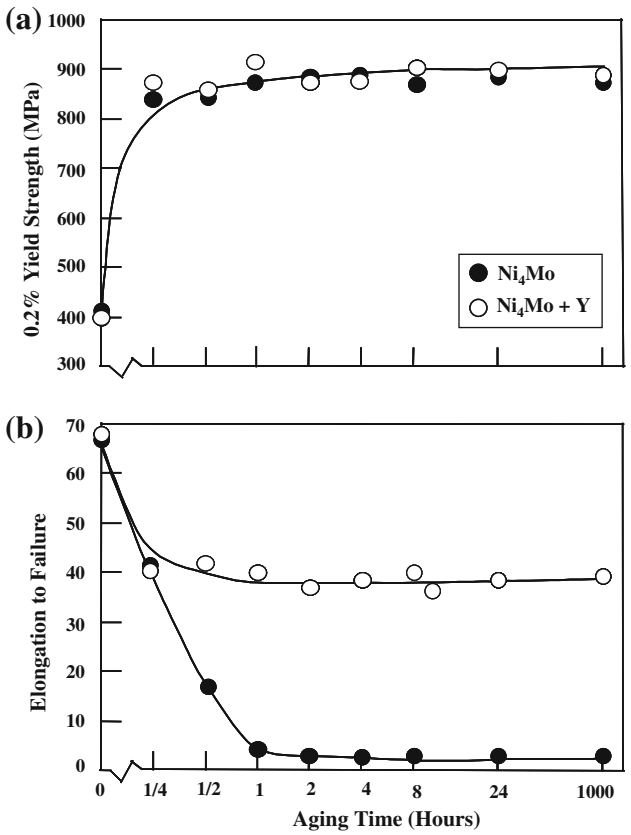

Fig. 3 Effect of aging time at 700 °C on the room-temperature tensile properties. **a** 0.2% yield strength. **b** Elongation to failure

could be related to the deformation mechanism as shown later.

Figure 3a shows the effect of thermal aging time up to 1000 h at 700 °C on the room-temperature 0.2% yield strength. It is observed that the undoped and doped Ni_4Mo exhibit similar behavior in that the yield strength is almost doubled relative to the as-quenched condition within the first 15 min of thermal aging reaching a value of about 850 MPa and then remains essentially unchanged with continued aging. However, the undoped alloy suffers an almost complete loss of ductility, while the doped alloy retains about 70% of the initial ductility corresponding to about 40% tensile elongation to failure as illustrated in Fig. 3b. The above observed differences in tensile properties are interpreted in terms of variation in the microstructure and deformation mechanism as explained below.

In the ordered state, both the doped and undoped alloys were almost fully ordered after 15 min of thermal aging at 700 °C with a volume fraction of Ni4Mo exceeding 95% as determined in an earlier study by X-ray diffraction analysis [19]. The crystallographic relationship between the parent fcc lattice and $D1_a$ superlattice of Ni_4Mo is shown in Fig. 4a as viewed along ⟨001⟩ direction. Only minor atoms rearrangement is involved in the fcc → $D1_a$ transformation resulting in the sequence of Mo/Ni/Ni/Ni/Ni/Mo/… on {420} planes and corresponding six crystallographically equivalent variants. This has an important implication on the deformation mechanism in the fully ordered state as shown later. During the early stages of thermal aging, nanoscale aligned arrays of ordered particles are observed in both the undoped and doped alloys as shown in the example of Fig. 4b. However, a considerable coarsening of Ni_4Mo occurs in the undoped alloy resulting in large platelets in the matrix and lamellar structure at the grain boundaries as shown in Fig. 4c. This behavior is known to occur in other alloy systems such as the Ni–V and Ni–Fe and is attributed to self-generated or strain-induced recrystallization to minimize the strain energy associated with the disorder-order transformation [20, 21]. The grain boundary structure shown in Fig. 4c is typical of a discontinuous ordering reaction generating alternating lamellae of Ni_4Mo (dark contrast) and Mo-depleted solid-solution (bright contrast). It is believed that because of the relatively low diffusivity of Mo, the localized solid-solution phase may exist in a state of metastable equilibrium for extended periods of time. This behavior could lead to highly localized deformation by slip within the Mo-depleted "soft" zones alongside grain boundaries explaining, at least partially, the observed loss of ductility. However, the doped alloy is found to exhibit a different behavior in that coarsening of Ni_4Mo particles and the grain boundary reaction are suppressed for at least 1000 h of aging maintaining a nanoscale structure as demonstrated in the dark-field image of Fig. 4d and e, respectively. Figure 4d is a dark-field image showing nanoparticles corresponding to one of the six

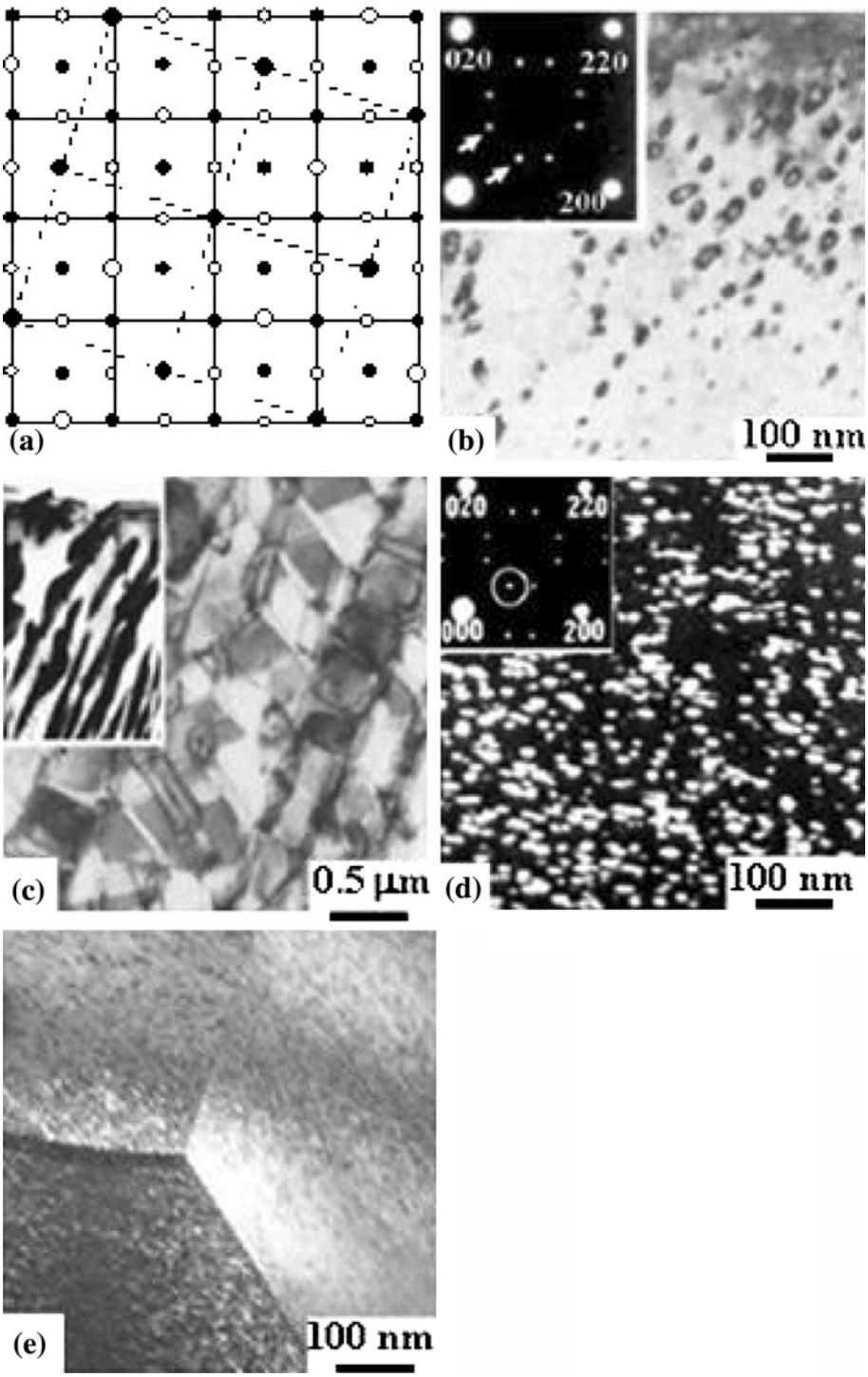

Fig. 4 Characteristic microstructural features of undoped and doped Ni_4Mo. **a** Crystallographic relationship between the parent fcc lattice (*solid lines*) and $D1_a$ superlattice (*dotted lines*) as viewed along the ⟨001⟩ direction (*large circles* represent Mo atoms and *small circles* represent Ni atoms; *black circles*: atoms at levels 0 and 1, *white circles*: atoms at level 1/2). **b** Bright-field TEM image of nanoparticles of Ni_4Mo after 5 min at 700 °C (no difference between undoped and doped alloys), the *inset* is ⟨001⟩ diffraction pattern showing $D1_a$ superlattice reflections. **c** Bright-field TEM image of large platelets on Ni_4Mo in the matrix of the undoped alloy after 1440 min at 700 °C; the *inset* shows the lamellar structure at a grain boundary. **d** Dark-field TEM image formed with a superlattice reflection in the inset showing one variant of nanoparticles of Ni_4Mo in the doped alloy after 1440 min at 700 °C. **e** Bright-field TEM image showing the absence of lamellar structure at original grain boundaries

crystallographically equivalent variants of the ordered phase. A low-magnification bright-field image is shown in Fig. 4e to illustrate the absence of the discontinuous ordering reaction at the original grain boundaries of the parent fcc phase. As can be seen, ordering occurred up to the original grain boundaries and each grain is divided into an aggregate of nanoscale ordered particles as exemplified in the dark-field image of Fig. 4e.

Although B is also found to improve the ductility of ordered Ni_4Mo alloys [22, 23], the microstructures of the Y-doped alloy is found to be similar to that of the B-doped alloy. However, the Y-doped alloy is found to have improved

thermal stability characteristics in that the desirable nanoscale ordered microstructure is maintained for longer exposure time at 700 °C (Fig. 3). In an earlier study of the undoped alloy and prior to the onset of the grain boundary reaction, e.g., 15 min of aging at 700 °C (see Fig. 3); a low strain hardening rate very similar to that of Fig. 2 was observed [24]. This indicated that this behavior is independent of doping but rather dependent upon the effect of ordering on the deformation mechanism demonstrated below.

Consistent with the deformation behavior of an fcc material having relatively low-stacking fault energy, the substructure is observed to contain slip lines with little tendency for cross slip as well as separated partial dislocations in the short-range ordered state (as-quenched) as shown in the example of Fig. 5a. However, in the long-range ordered state, deformation is found to predominantly occur by twinning on the {111} planes of the parent fcc lattice as demonstrated in Fig. 5b, which could explain the lower strain hardening rate relative to the short-range ordered condition (Fig. 2). Also, twinning is found to preserve ordering as demonstrated in Fig. 5c and therefore, it becomes an energetically favorable deformation mechanism in the long-range ordered state. This could be understood in terms of the crystallographic features of the $D1_a$ superlattice as shown in Fig. 5d. Although all the {111} ⟨110⟩ slip systems are suppressed, eight of the respective 12 twinning systems {111} ⟨112⟩ remain energetically favorable.

Although the exact mechanism responsible for the beneficial effect of Y remains to be established, it is believed to be related, at least partially, to its tendency to segregate at grain boundaries. Other useful intermetallic properties retained in the doped Ni_4Mo alloy are described below.

A low coefficient of thermal expansion is important in many applications requiring closer dimensional tolerance. Although doping with yttrium is found to have no measurable effect, a lower coefficient is observed in the ordered state as illustrated in Fig. 6a as expected of an ordered structure. For comparative purposes, Fig. 6a also shows the value corresponding to the nickel steel or Invar well known for it very low coefficient of thermal expansion.

Ni–Mo alloys containing more than 15 wt% Mo are known for their high corrosion resistance in reducing media particularly hydrochloric acid [25]. Figure 6b shows comparative corrosion rates in boiling 20% HCl. As can be seen, the Y-doped Ni_4Mo has a slightly higher corrosion rate in comparison with the short-range ordered condition (as-quenched). However, the rate remains well within the acceptable level (0.1–1.3 mm/year) [24]. It is to be noted that although the high volume fraction of boundaries/

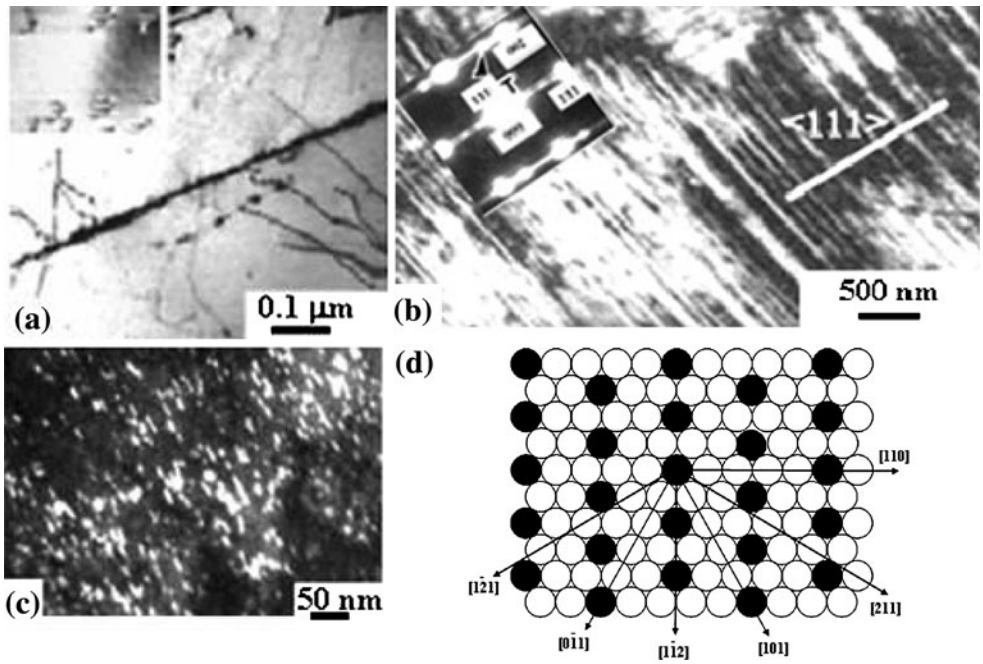

Fig. 5 Comparative deformation behavior: **a** Bright-field TEM image showing tensile deformation substructure in the short-range ordered condition (as-quenched) corresponding to 0.05 strain; the *inset* shows separated partial dislocations. **b** Bright-field TEM image and corresponding ⟨110⟩ diffraction pattern showing {111} deformation twins corresponding to 0.15 strain in the doped alloy (aged 1440 min at 700 °C). **c** Dark-field TEM image showing ordered particles within the deformation twins. **d** A schematic illustration of the atoms arrangement on a {111} plane showing the slip and twin systems in the $D1_a$ superlattice

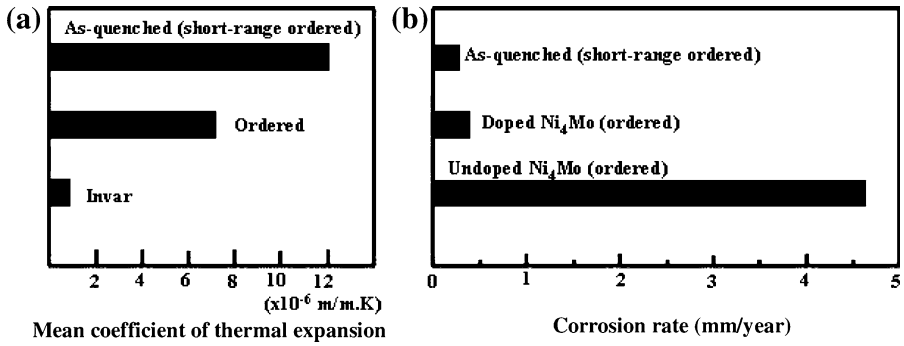

Fig. 6 Comparative physical and chemical properties: **a** Mean coefficient of thermal expansion in the temperature range of 20–540 °C. **b** Corrosion rate in boiling 20% hydrochloric acid

interfaces in the nanocrystalline superlattice is expected to increase the corrosion rate, at least some of this could be offset by the atomic order. The rather high corrosion rate of the undoped Ni_4Mo (about 4.6 mm/year) could be attributed to the presence of localized Mo-depleted zones alongside the grain boundaries resulting from the discontinuous reaction as described earlier.

Conclusion

It is concluded from this study that nanocrysalline Ni_4Mo alloy with ultrahigh strength and high ductility can be synthesized by small but critical additions of Y and simultaneously retaining other useful physical and chemical properties of intermetallic compounds. Transformation into the $D1_a$ superlattice of Ni_4Mo is found to favor twinning rather than slip as the predominant deformation mechanism.

Acknowledgement It is a pleasure to acknowledge the continued support of King Fahd University of Petroleum & Minerals.

References

1. Valiev RZ, Estrin Y, Horita Z, Langdon TG, Zehetbauer MZ, Zhu YT (2006) J Met 58(4):33
2. Valiev RZ (2004) Nat Mater 3:511
3. Valiev RZ, Isiamgaliev RK, Alexandrov IV (2000) Prog Mater Sci 45:103
4. Valiev RZ, Alexandrov IV, Zhu YT, Lowe TC (2002) J Mater Res 17(1):5
5. Zhu YT, Liao XZ (2004) Nat Mater 3:351
6. Koch CC (2003) Scripta Mater 49(7):657
7. Cahn RW (2001) Contemp Phys 42:365
8. Tawancy HM, Aboelfotoh MO (2009) Mater Sci Eng A 500(1–2): 188
9. Tawancy HM, Aboelfotoh MO (2008) Scripta Mater 59(8):846
10. Gschneidner KA, Ji M, Wang CZ, Ho KM, Russell AM, Mudryk Y, Becker AT, Larson JL (2009) Acta Mater 57:5876
11. Gshneidner KA, Russell A, Pecharsky A, Morris J, Zhang Z, Logarsso T, Hsu C, Lo Y, Yiying A, Slager A, Kesse D (2003) Nat Mater 2:587
12. Tawancy HM, Aboelfotoh MO (1987) Phys Status Solidi A 99(2):461
13. Rothman MF, Tawancy HM (1989) Low thermal expansion alloy. US Patent No. 4,818, 486
14. Tawancy HM (2009) Corrosion resistant nickel base alloy. US patent No. US2009004043-A
15. Brooks CR, Spruiel JEl, Stansbury EE (1984) Intern Met Rev 29:210
16. Nesbit LA, Laughlin DE (1980) Acta Metall 28:989
17. Hata S, Shindo D, Mitate T, Kuwano N, Matsumura S, Oki K (2000) Micron 31:533
18. Allen SM, Cahn JW (1972) Acta Metall 20(3):423
19. Tawancy HM, Alyousef FK (2007) J Mater Sci 42(21):9121. doi: 10.1007/s10853-007-2056-1s
20. Tanner LE, Leamy HJ (1974) In: Warlimont H (ed) Order-disorder transformations in alloys. Springer-Verlag, New York, p 180
21. Snyder WB, Brooks CR (1970) In: Kear BH, Sims CT, Stoloff NS, Westbrook JH (eds) Ordered alloys: structural applications and physical metallurgy. Claitor's publishing division, Baton Rouge, Louisiana, p 275
22. Wright JL, Zhu JH, Horton JA, Heatherly L Jr (2001) Intermetallics 9:1021
23. Tawancy HM (1991) Metall Trans A 22(12):3067
24. Tawancy HM, Abbas NM (1989) J Mater Sci 24:1845. doi: 10.1007/BF01105714
25. Hodge FG (1983) In: Schweitzer PA (ed) Corrosion and corrosion protection handbook. Marcel Dekker, New York, NY, p 65